Williams, Immanuel; Belahcen, Anouar; Kulkarni, Shrikrishna V.

An Investigation into Permanent Magnet Hysteresis Losses in Reverse-salient Permanent Magnet Synchronous Motors

Published in:
2023 IEEE 32nd International Symposium on Industrial Electronics, ISIE 2023 - Proceedings

DOI:
10.1109/ISIE51358.2023.10228137

Published: 01/01/2023

Document Version
Peer-reviewed accepted author manuscript, also known as Final accepted manuscript or Post-print

Please cite the original version:
Williams, I., Belahcen, A., & Kulkarni, S. V. (2023). An Investigation into Permanent Magnet Hysteresis Losses in Reverse-salient Permanent Magnet Synchronous Motors. In *2023 IEEE 32nd International Symposium on Industrial Electronics, ISIE 2023 - Proceedings* (Proceedings of the IEEE International Symposium on Industrial Electronics; Vol. 2023-June). IEEE. https://doi.org/10.1109/ISIE51358.2023.10228137

An Investigation into Permanent Magnet Hysteresis Losses in Reverse-salient Permanent Magnet Synchronous Motors

Immanuel Williams
Department of Electrical Engineering and Automation
Aalto University
Espoo, Finland, and
Department of Electrical Engineering
Indian Institute of Technology, Bombay
Mumbai, India
immanuelw2000@gmail.com

Anouar Belahcen
Department of Electrical Engineering and Automation
Aalto University
Espoo, Finland
anouar.belahcen@aalto.fi

Shrikrishna V. Kulkarni
Department of Electrical Engineering
Indian Institute of Technology, Bombay
Mumbai, India
svk@ee.iitb.ac.in

***Abstract*—Hysteresis losses occurring in Permanent Magnets can be significant when the operating point of the magnets crosses the B-axis (H = 0 line), resulting in large minor loops. In traditional Interior Permanent Magnet Synchronous Motors, it has been extensively studied and observed that these losses aren't significant under regular operating conditions. The conditions responsible for these losses may exist under the regular operating conditions of a Reverse-salient Permanent Magnet Synchronous Motor for which, no discussion on these kinds of losses has been done before. This paper bridges the aforementioned knowledge gap by investigating the existence of such losses in a Reverse-salient Permanent Magnet Synchronous Motor to understand if there is a cause for concern.**

***Index Terms*—Permanent Magnets, Hysteresis Losses, Reverse-salient Permanent Magnet Synchronous Motors**

I. Introduction

Core losses occurring in the rotor of a Permanent Magnet Synchronous Motor (PMSM) are limited mainly due to the fact that it rotates at the same speed as the fundamental component of the stator MMF. Irregularities in the geometry like rotor saliency or arrangement of Permanent Magnets (PMs) buried inside an Interior PMSM (IPMSM) rotor along with harmonic content from the converter feeding the motor can generate magnetic fields that rotate at speeds that are integer multiples of the rotor speed [1]. In the rotor reference frame, these fields would then be time-variant and not static which leads to losses.

The dominant losses occurring in the Permanent Magnets (PMs) are eddy current losses and different calculation techniques have been suggested to calculate these losses more effectively [2], [3]. However, it has been shown in [4] that PM hysteresis losses can be just as great as eddy current losses. These losses get aggravated due to the operating point tracing significant minor loops while crossing the B-axis [5]. According to [6], it is possible to limit such losses if the IPMSM is designed to limit the swing in PM flux density.

The Reverse-salient PMSM (RSPMSM) is a class of IPMSM that is designed in a way such that the saliency ratio is less than 1 which allows the motor to be operated in a flux-amplifying mode of operation which increases the torque output below the base speed [7], [8]. This and a wide constant-power zone of operation make the RSPMSM an attractive choice for the Electric Vehicle (EV) industry. However, the flux-amplifying mode of operation can put the PMs at risk of incurring hysteresis losses.

This paper investigates the existence of such losses in an RSPMSM. Section II gives a brief overview of PM Hysteresis Losses and Section III describes the theory behind operating an RSPMSM as well as its advantages. Section IV outlines the strategy to estimate PM hysteresis losses in an RSPMSM, and Section V discusses the results obtained from the estimates obtained.

II. A Brief Review on PM Hysteresis Losses

It has been observed in [5], [6], [9] that the minor loop traced is much larger than the situation when the operating point of the PM doesn't cross the B-axis. While the physics behind the origin of this phenomenon is not clear, [5] ascribes this to the presence of magnetically soft areas within a hard magnetic material. Because of these magnetically soft areas, the complete hysteresis loop of a PM material can be thought of as a combination of a major loop and a small minor loop centered at a point on the B-axis where this phenomenon is observed.

It can be inferred that minor loops like loop 1 in Fig. 1 will have larger hysteresis energy than minor loops like loop 2. It has been reported in Fig. 5 of [5] that for NdFeB magnets,

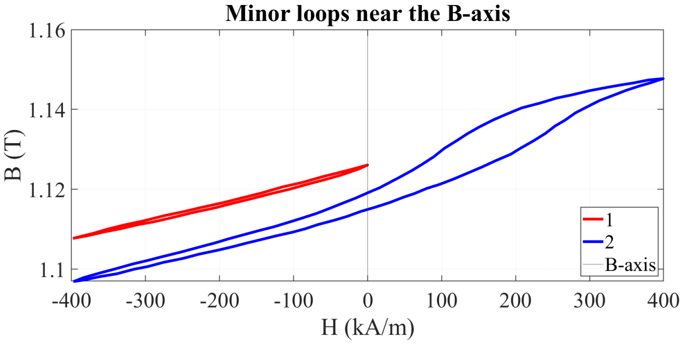

Fig. 1: Minor loops in a NdFeB magnet near the B-axis (H = 0 curve). Reproduced using data from Fig. 5 of [5]. Here, H is the applied field and not the intrinsic field of the material

the smallest minor loop that crosses the B-axis has an energy density of 145 J/m^3 whereas the largest such loop that does not cross the B-axis has an energy density of 73 J/m^3. Thus a sizeable proportion of losses occurring in PMs can be attributed to these minor loops as long as the B-axis is crossed. In the next section, the possibility of such a situation arising will be discussed in the case of an RSPMSM while describing the theory behind its operation and its advantage over a conventional IPMSM.

III. Operating Principles and Advantages of an RSPMSM over a Conventional IPMSM

The expressions for the electromagnetic torque T_{em} and supply voltage V_s in a PMSM are given by:

$$T_{em} = \frac{3}{4} P i_q (\lambda_m + (L_d - L_q) i_d) \tag{1}$$

$$V_s = \omega_e \sqrt{(L_q i_q)^2 + (L_d i_d + \lambda)^2} \tag{2}$$

Here, P is the number of poles, i_d and i_q are the d-axis and q-axis currents respectively, L_d and L_q are the d-axis and q-axis inductances respectively, λ_m is the magnet flux linkage, and ω_e is the electrical angular frequency which is given by $\omega_e = \pi P N_{rot}/60$ where N_{rot} is the mechanical speed of the rotor when expressed in rpm. In this analysis, core saturation as well as the core and copper losses are ignored. The governing equations given in Sections IIA and IIIA of [8] are solved again due to a mistake in equation 8 of [8] which results in a dimensionally inconsistent expression for i_d. In this work, the governing equations are solved by normalizing quantities using a suitable base, and new equations consisting of per-unit (p.u.) values of the original quantities are solved.

The saliency ratio of a PMSM is given by $\rho = L_q/L_d$. Define the inductance base $L_b = \lambda/I_{max}$ and the torque base $T_b = 3P\lambda I_{max}/4$, where I_{max} is the maximum stator current. The p.u. values of the d-axis inductance, electromagnetic torque, i_d, and i_q are $L_d^* = L_d/L_b$, $T_{em}^* = T_{em}/T_b$, $i_d^* = i_d/I_{max}$ and $i_q^* = i_q/I_{max}$ respectively. (3) is (1) rewritten using the p.u. equivalents of the corresponding quantities.

$$T_{em}^* = i_q^*(1 + (1-\rho) L_d^* i_d^*) \tag{3}$$

$$(i_q^*)^2 + (i_d^*)^2 = 1 \tag{4}$$

(4) is an additional constraint that has to be satisfied by the p.u. currents. Below the base speed N_{base}, when the Maximum Torque Per Ampere (MTPA) control scheme is in effect, $i_{d,M}^*$ (i_d^* which maximizes T_{em}^*) is given by (5) (for $\rho \neq 1$).

$$i_{d,M}^* = \frac{-1 + \sqrt{(1 + 8(1-\rho)^2 (L_d^*)^2)}}{4(1-\rho) L_d^*} \tag{5}$$

For $N_{rot} > N_{base}$, (2) can be recast into (6) while expressing all quantities in their p.u. equivalents. In (7), a new parameter e^* is defined, $\omega_{e,M} = \pi P N_{base}/60$, $n^* = N_{rot}/N_{base}$ is the p.u. speed, and e_M^* is obtained by substituting $i_{d,M}^*$ in (7). This follows from the fact that the limiting stator voltage is attained at N_{base} which is the highest speed at which the MTPA control strategy is still valid. Finally, the output power P_{out} is obtained using $P_{out} = \pi T_{em} N_{rot}/30$. Table I enlists the parameters of a conventional IPMSM and an RSPMSM with similar design specifications like rotor and stator diameters that have been compared in [8]. Here, $I_{rat} = I_{max}/\sqrt{2}$ is the rated current.

$$e^* = \frac{e_M^*}{(\omega_e/\omega_{e,M})^2} = \frac{e_M^*}{(N_{rot}/N_{base})^2} = \frac{e_M^*}{(n^*)^2} \tag{6}$$

$$e^* = (1-\rho^2)(L_d^* i_d^*)^2 + 2 L_d^* i_d^* + 1 + (\rho L_d^*)^2 \tag{7}$$

PMSM Parameters	Conventional IPMSM	RSPMSM
I_{rat}	8.95 A	8.95 A
L_d	31.82 mH	32.72 mH
L_d^*	0.86	1
N_{base}	1200 rpm	1200 rpm
ρ	0.9	1.1

TABLE I: Parameters for PMSM comparison

It can be observed from Fig. 3a that the RSPMSM can deliver more torque than the conventional IPMSM at the same operating speed beyond the base speed and this can be explained by Fig. 2b where one can observe that i_q^* of an RSPMSM is larger than that of a traditional IPMSM. From Fig. 2a, the RSPMSM can also operate in the flux-amplifying mode even beyond the base speed and when it does enter into the flux-weakening mode, i_d^* is smaller in magnitude than that of a conventional IPMSM. This confers the advantages of a wider constant power speed region which is clearly evident in Fig. 3b and a lesser risk of demagnetization due to the applied stator MMF, two improvements over the conventional IPMSM which make the RSPMSM, a viable candidate in the EV industry [7], [8]. However, the flux-amplifying mode of operation can push the operating point of the magnet near the B-axis of the magnet and the presence of slot and permeance harmonics can result in PM hysteresis losses. The strategy used to estimate these losses will be explained in the next section along with the example machine used for this purpose.

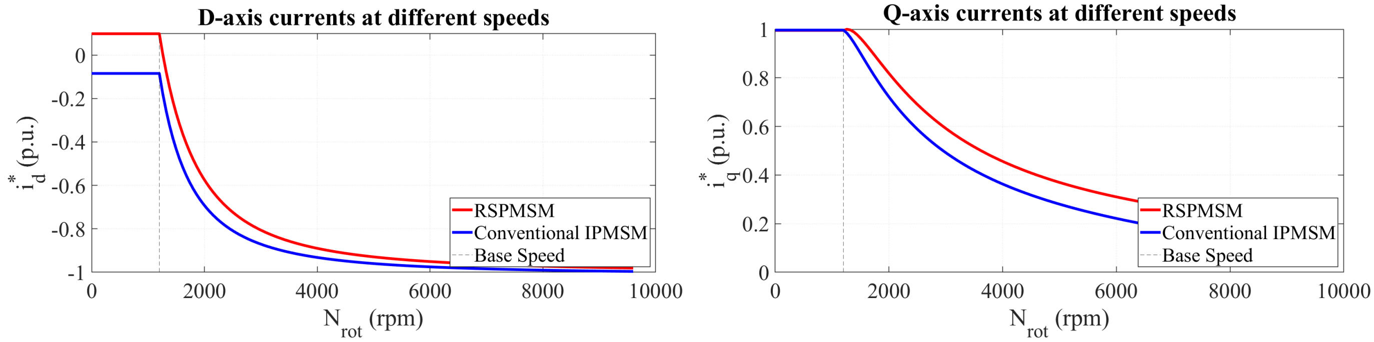

(a) (b)

Fig. 2: Current-Speed curves of RSPMSM and conventional IPMSM. (a) d-axis (b) q-axis

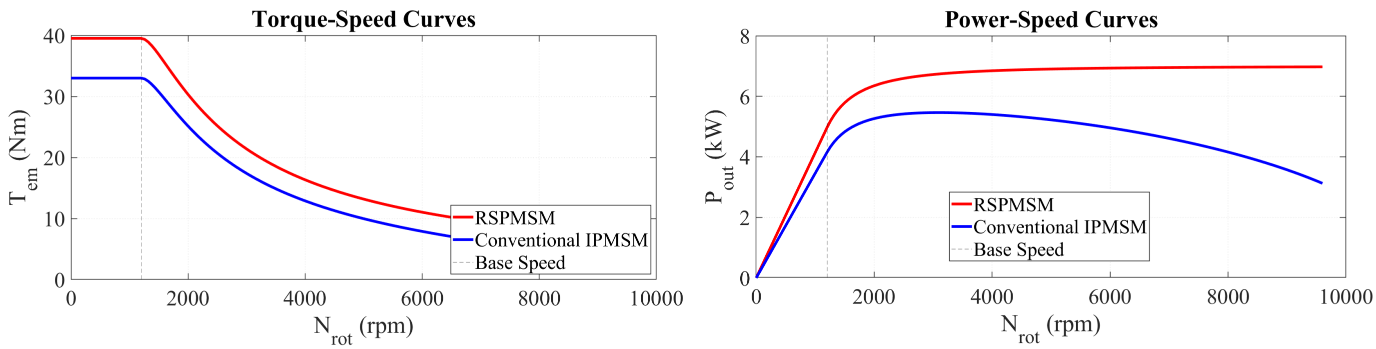

(a) (b)

Fig. 3: (a) Torque-Speed and (b) Power-Speed curves of RSPMSM and conventional IPMSM

IV. Methodology for Calculating PM Hysteresis Losses in an Example Machine

Parameter	Unit	Value
Stator Outer Diameter	mm	169
Rotor Outer Diameter	mm	100
Minimum Air-gap Length	mm	0.8
Axial Length	mm	100
Thickness of Magnetic Bridges	mm	0.75
Thickness of PMs	mm	3.6
Length of PMs	mm	6
Radius of Q-axis flux barrier	mm	25
Angle of PM V shape	deg	56.8
Shaft and Core Material	N/A	DW465-50

TABLE II: Important RSPMSM design parameters

Fig. 4 describes the geometry of an RSPMSM which is simulated on COMSOL Multiphysics using a combination of the Rotational Magnetic Machinery (RMM) and the Domain ODEs and DAEs (DODEs) physics modules (ODEs: Ordinary Differential Equations and DAEs: Differential-Algebraic Equations). Table II presents an overview of some of the important machine parameters that are fed to the software for designing the geometry, of which, the Q-axis flux barrier radius and the PM V-shape angle are taken from [10] and the other parameters are taken from [7].

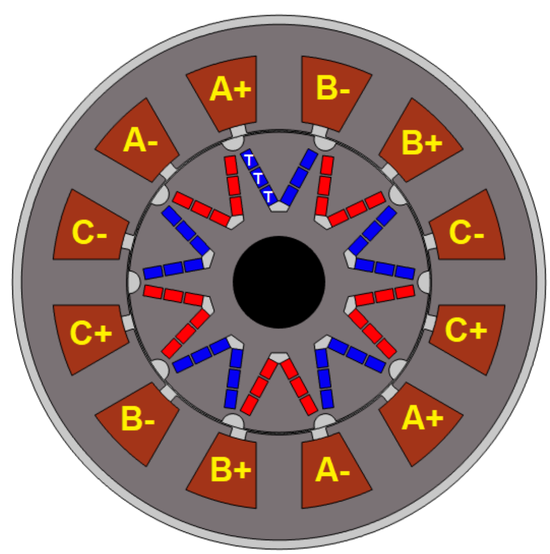

Fig. 4: Geometry of the test RSPMSM (The magnets marked with the white letter T are the Test Magnets)

The PMs (red and blue corresponding to different magnetization directions) are modeled with a remanent flux density model in the RMM physics module. For this model, the remanent flux density B_r is set to 1.1 T and the recoil permeability μ_{rec} is set to 1.07 in accordance with the data given in Table I of [5]. The windings are excited with a 3-phase balanced, sinusoidal current source with peak amplitude 40 A while the rotor is rotated at a constant speed of 1200 rpm. The simulation is made to run for a time period corresponding to three rotor rotations.

In [5], a test magnet is divided into a large number of small segments and the PM hysteresis loss is estimated by evaluating the peak-to-peak ripple in the PM flux density along the direction of magnetization. The recoil permeability of the PMs is held constant during FEM simulations. The losses are post-processed by considering this ripple while also checking if the remanent flux density is being crossed intermittently. For a given segment, if the ripple in the PM flux density is in the range or higher than what was measured and reported, the hysteresis energy is taken to be equal to the hysteresis energy corresponding to the measured minor loops and the overall hysteresis loss is calculated by summing up the hysteresis losses over all segments.

The geometry is meshed by setting the maximum element size to 1 mm and the minimum size to 0.01 mm which results in a mesh with 36968 vertices, 72356 triangles, and 5750 edge elements. Due to PM rotation, a coordinate transformation has to be applied to observe flux density in the direction of magnetization. As the rotor rotates at a constant speed, the PM flux density in the test magnets along the magnetization direction (B_{mag}) is evaluated using the following equation:

$$B_{mag} = B_x \cos(\omega_{mech} t + \theta_0) + B_y \sin(\omega_{mech} t + \theta_0) \quad (8)$$

Where B_x and B_y are the x and y components of the magnetic flux density vector, ω_{mech} is the mechanical angular speed of rotation, t is the time, and θ_0 is the angle that the direction of magnetization of the test magnets makes with the x-axis at $t = 0$. Fig. 4 depicts the rotor position at $t = 0$ and using that, it can be shown that $\theta_0 = 28.4^o$ which is half the PM V shape angle. Then, a subroutine for detecting and storing the maximum and minimum values of PM flux density over time (B_{max} and B_{min} respectively) is deployed using the DODE physics module.

In the case of NdFeB, six minor loops were recorded in Fig. 5 of [5] of which three do not cross the remanent flux density. Let ΔB and E_h denote the width and hysteresis energy associated with a minor loop respectively. The loss data corresponding to NdFeB given in [5] is fitted to $E_h = k_h(\Delta B)^2$ curves. Curve fitting yields two constants $k_{h,1}$ and $k_{h,2}$ in which subscript 1 corresponds to the case where the minor loop does not cross the B-axis and subscript 2 corresponds to the other case. This is inspired by the approaches of Bertotti and Steinmetz [11] in which the hysteresis energy associated with a major loop is considered proportional to the square of the peak magnetic flux density of the loop. In this case, the BH loops are no longer major loops but they are minor loops and therefore a more prudent choice is to use ΔB.

The B_{max} and B_{min} values in a small segment of the PM are used to calculate the width of the minor loop that crosses the B-axis with an equal extent on either side by using, $\delta B = \max(0, 2 \times \min(B_{max} - B_r, B_r - B_{min}))$. This formula in itself also checks for the existence of such a loop because it can be seen that the only way for such a loop to exist and have some finite width is when $B_{min} < B_r < B_{max}$. In order to calculate the total hysteresis energy, the energy contribution from this loop as well as the energy contribution from the remaining smaller loop that does not cross the B-axis has to be added. The width of the remaining smaller loop can be obtained by subtracting δB from the total loop width $\Delta B = B_{max} - B_{min}$. Next, the following formula is used to estimate the hysteresis energy:

$$E_h = k_{h,1}(\Delta B - \delta B)^2 + k_{h,2}(\delta B)^2 \quad (9)$$

Finally, the hysteresis energy divided by the period of the PM flux density waveform gives the losses. Since this time period is the inverse of double the mechanical frequency of rotation, the volumetric hysteresis loss density is calculated using $P_{h,V} = E_h N_{rot}/30$. To compare this with the volumetric loss density due to eddy currents, loss calculation with a resistive heating model has been enabled for the PMs in the RMM interface and the electrical resistivity of NdFeB is set to 150 $\mu\Omega cm$ according to [12].

In addition to this, the average, maximum, and minimum flux density values along the magnetization direction are evaluated over the test magnets, at a given instant of time. The waveforms depicting the time-variation of these values are then plotted from t = 0.09 s to t = 0.15 s. The calculated volumetric loss density due to hysteresis effects is integrated over the test magnets, which is then multiplied by twice the number of poles (twice because the test magnets form one half of a pole) to determine the PM hysteresis loss.

V. Results and Discussion

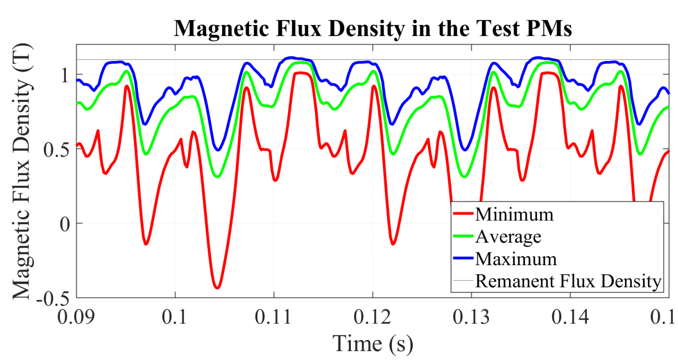

Fig. 5: Time variation of Flux Density in the Test Magnets

Fig. 5 depicts the PM Flux Density variation in the Test Magnets and from the simulation, it is observed that the RSPMSM delivers nearly 5.68 kW with 89.5 % efficiency.

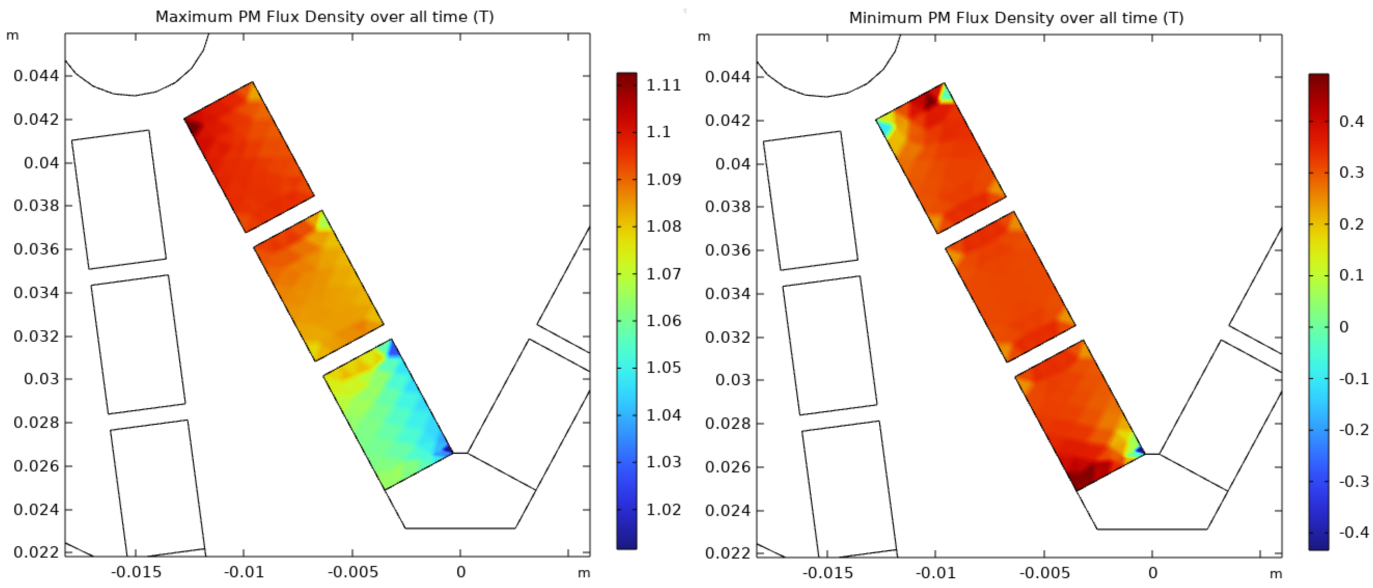

(a) (b)

Fig. 6: (a) Maximum and (b) Minimum PM flux-density values in the Test Magnets

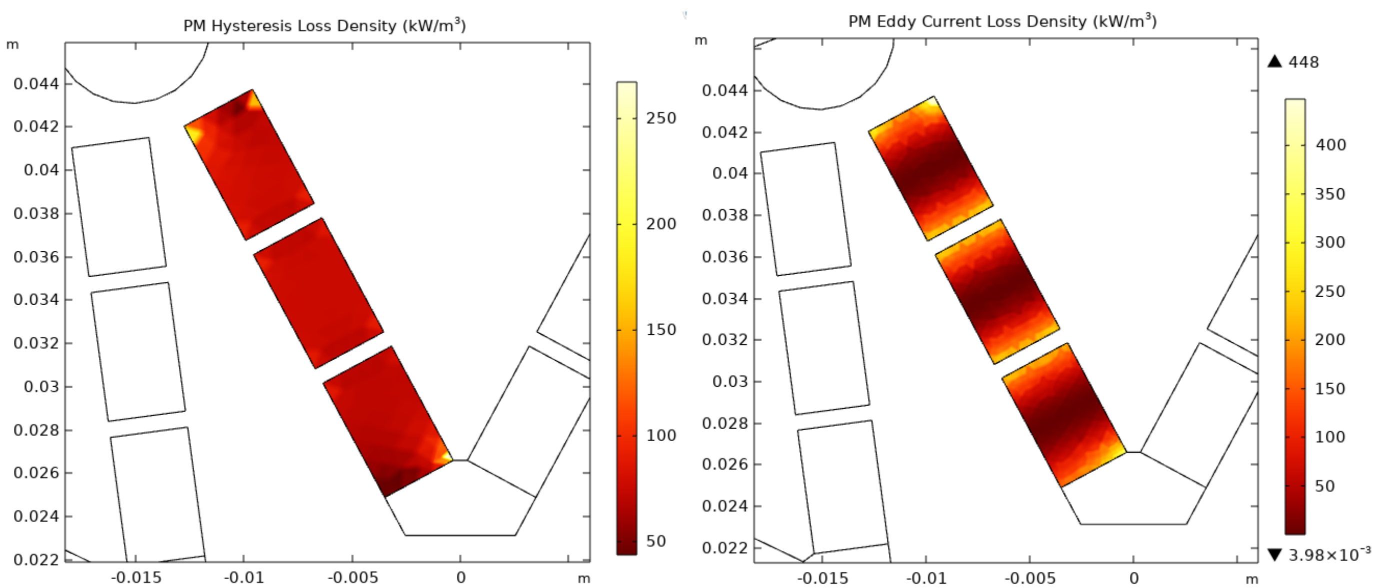

(a) (b)

Fig. 7: (a) Hysteresis and (b) Eddy-Current losses occurring in the Test Magnets

Figs. 6a and 6b depict the maximum and minimum values of the PM flux density recorded over the entire simulation period. In Fig. 5 of [5], the minor loops that do not cross the remanent flux density have a very small swing therefore, the losses themselves are very small and the assumption that the magnetization of the PMs is invariant is valid, which is essentially why PM hysteresis losses are ignored in general. However, Figs. 5, 6a, and 6b suggest the existence of significant hysteresis losses due to a massive swing in the PM flux density alone. In addition, the PM flux density exceeds the remanent flux density near some edges which would further increase the losses. These factors coupled with the paucity of data on PM hysteresis losses are the reasons why the approach given in [5] is extended using the loss calculation model given by (9).

Figs. 7a and 7b depict the hysteresis and eddy-current volumetric loss densities respectively. Unlike the eddy-current losses which are more prominent over all edges of the magnets parallel to the magnetization direction, significant hysteresis loss is observed at three different places of which, only one of those corresponds to regions with a huge swing as well as $B_{min} < B_r < B_{max}$ whereas the other two regions have a significant loss due to a huge swing in the magnetic field alone. This is in accordance with [1] which explains that PM losses are more prominent near the edges and are not evenly distributed over the bulk of the material. It is also observed that the PM hysteresis losses are of comparable magnitude to the eddy current losses. The total PM hysteresis loss evaluates to 9.928 W which is 0.17 % of the nominal power output.

VI. Conclusion and Future Work

In this paper, the existence of PM hysteresis losses occurring in RSPMSMs is investigated and it is observed that these losses are significant not only because of a huge swing in the PM flux density but also because of the operating condition which causes the PM flux density to exceed the remanent flux density. The hysteresis loss density occurring near the edges of the PMs is indeed comparable with the eddy current loss density, similar to the observations reported in [4]. Although the absolute value of the computed loss is insignificant, the loss density occurring at the edges can be appreciable enough to cause problems due to an increase in temperature. The influence of these losses on the thermal behavior of the PMSM that affects the electromagnetic behavior [13], in turn, is something that has to be dealt with in future work with an aim to understand if these losses can be reduced at an early design stage and if a material characterization model is needed to capture this phenomenon. As this was an investigative analysis, no experimental work is presented and the required data is taken from literature as any experimental analysis to determine and characterise PM materials specifically for these kinds of hysteresis losses requires a lot of planning and effort.

References

[1] J. R. Hendershot and T. J. E. Miller, "Design of Brushless Permanent -Magnet Machines", Motor Design Books LLC, Florida, 2010.

[2] R. Sahu, P. Pellerey, and K. Laskaris, "Eddy Current Loss Model Unifying the Effects of Reaction Field and Non-Homogeneous 3-D Magnetic Field," in *IEEE Transactions on Magnetics*, vol. 56, no. 2, pp. 1-4, Feb. 2020, Art no. 7508404, doi: 10.1109/TMAG.2019.2953110.

[3] J. Pyrhonen, H. Jussila, Y. Alexandrova, P. Rafajdus, and J. Nerg, "Harmonic Loss Calculation in Rotor Surface Permanent Magnets—New Analytic Approach," in *IEEE Transactions on Magnetics*, vol. 48, no. 8, pp. 2358-2366, Aug. 2012, doi: 10.1109/TMAG.2012.2190518.

[4] A. Fukuma, S. Kanazawa, D. Miyagi, and N. Takahashi, "Investigation of AC loss of permanent magnet of SPM motor considering hysteresis and eddy-current losses," in *IEEE Transactions on Magnetics*, vol. 41, no. 5, pp. 1964-1967, May 2005, doi: 10.1109/TMAG.2005.846282

[5] I. Petrov, D. Egorov, J. Link, R. Stern, S. Ruoho, and J. Pyrhönen, "Hysteresis Losses in Different Types of Permanent Magnets Used in PMSMs," in *IEEE Transactions on Industrial Electronics*, vol. 64, no. 3, pp. 2502-2510, March 2017, doi: 10.1109/TIE.2016.2548440

[6] J. Pyrhönen et al., "Hysteresis Losses in Sintered NdFeB Permanent Magnets in Rotating Electrical Machines," in *IEEE Transactions on Industrial Electronics*, vol. 62, no. 2, pp. 857-865, Feb. 2015, doi: 10.1109/TIE.2014.2354597.

[7] X. Zhao, B. Kou, C. Huang, and L. Zhang, "A Reverse-Salient Permanent Magnet Synchronous Motor For Electric Vehicles Considering Operating Conditions," in *IEEE Transactions on Energy Conversion*, 2022, doi: 10.1109/TEC.2022.3213571.

[8] X. Zhao, B. Kou, and C. Huang, "A Reverse-Salient Permanent Magnet Synchronous Motor and Its dq-Axis Current Distribution Laws," in *IEEE Transactions on Industrial Electronics*, vol. 70, no. 4, pp. 3337-3347, April 2023, doi: 10.1109/TIE.2022.3174281.

[9] S. Ruoho, E. Dlala, and A. Arkkio, "Comparison of Demagnetization Models for Finite-Element Analysis of Permanent-Magnet Synchronous Machines," in *IEEE Transactions on Magnetics*, vol. 43, no. 11, pp. 3964-3968, Nov. 2007, doi: 10.1109/TMAG.2007.906749.

[10] Zhao, X.; Kou, B.; Huang, C.; Zhang, L. Optimization Design and Performance Analysis of a Reverse-Salient Permanent Magnet Synchronous Motor. Machines 2022, 10, 204. https://doi.org/10.3390/machines10030204

[11] Krings, andreas & Soulard, Juliette. (2010). Overview and Comparison of Iron Loss Models for Electrical Machines. Journal of Electrical Engineering. 10. 162-169.

[12] CHARACTERISTICS OF NDFEB MAGNETS. Online Website by Bunting E-Magnets. URL: https://e-magnetsuk.com/introduction-to-neodymium-magnets/characteristics-of-ndfeb-magnets/

[13] S. Ruoho, J. Kolehmainen, J. Ikaheimo, and A. Arkkio, "Interdependence of Demagnetization, Loading, and Temperature Rise in a Permanent-Magnet Synchronous Motor," in *IEEE Transactions on Magnetics*, vol. 46, no. 3, pp. 949-953, March 2010, doi: 10.1109/TMAG.2009.2033592.